Ion acceleration at dipolarization fronts associated with interchange instability in the magnetotail

Chao Sun[1], Yasong Ge[2], Haoyu Lu[1,3]

[1]*School of Space and Environment, Beihang University, Beijing, 100191, China (lvhy@buaa.edu.cn)*

[2]*Institute of Geology and Geophysics, Chinese Academy of Sciences, Beijing, 100029, China*

[3]*Lunar and Planetary Science Laboratory, Macau University of Science and Technology - Partner Laboratory of Key Laboratory of Lunar and Deep Space Exploration, Chinese Academy of Sciences, Macau, 519020, China*

Abstract It has been confirmed that dipolarization fronts (DFs) can be a result from the existence of interchange instability in the magnetotail. In this paper, we used a Hall MHD model to simulate the evolution of the interchange instability, which produces DFs on the leading edge. A test particle simulation was performed to study the physical phenomenon of ion acceleration on DF. Numerical simulation indicates that particles, with 90-degree pitch angle and initially satisfying the initial power law energy distribution $F \sim (1 + h/\kappa T_0)^{-\kappa-1}$ ($\kappa = 5$, $T_0 = 1.5\, keV$ and h from 1 keV to 10 keV), move towards the earthward and dawnward and

then drift to the tail. The DF-reflected ion population on the duskside appears earlier as a consequence of the asymmetric Hall electric field. Ions, with dawn-dusk asymmetric semicircle behind the DF, may tend to be accelerated to a higher energy (>6keV). These high-energy particles are eventually concentrated in the dawnside. Ions experience effective acceleration by the dawnward electric field E_y while they drift through the dawn flank of the front towards the tail.

Introduction

Earthward moving high-speed plasma flows, which are called bursty bulk flows (BBFs), play a vital important role in carrying significant amounts of mass, energy, and magnetic flux from the reconnection region to the near-Earth magnetotail (Angelopoulos et al., 1994). BBFs are often accompanied with a strong (~10nT), abrupt (several seconds), transient enhancement of the magnetic field component Bz in the leading part, known as a dipolarization front (DF) (Nakamura et al., 2009; Sergeev et al.,2009; Fu et al., 2012a). Ahead of the DF, a minor Bz dip usually be observed by THEMIS and MMS (Runov et al., 2009; Schmid et al., 2016), which may be typically interpreted as strong diamagnetic currents caused by a plasma pressure drop over the front or magnetic flux tube or transient reconnection (Kiehas et al., 2009; Ge et al., 2011; Schmid et al., 2011). Simulations have suggested that the magnetic energy would be transferred to plasma on the DF layer in the Bz dip region ahead of trailing fronts (Lu et al., 2017). Many of studies show that the passage of a magnetic island (Ohtani et al., 2004), jet braking (Birn et al., 2011), transient reconnection (Sitnov et al., 2009; Fu et al., 2013), and/or the interchange/ballooning instability (Guzdar et al., 2010; Pritchett and Coroniti, 2013) may account for DF generation. Both Cluster and MMS observed that DFs propagate not only earthward but also tailward, since the fast-moving DFs are compressed and reflected, three quarters of the

DFs propagate earthward and about one quarter tailward (Zhou et al., 2011; Nakamura et al., 2013; Huang et al., 2015; Schmid et al., 2016). Spacecraft observations showed that the sudden energy increase in charged particle fluxes at DFs from tens to hundreds of keV in the magnetotail (Runov et al., 2011; Zhou et al., 2010; Fu et al., 2011; Li et al., 2011; Artemyev et al., 2012). A series of studies have been conducted to understand the signatures of DFs and particles, as well as the particle acceleration mechanisms on the DFs. Li et al., (2011) studied the force balance between the Maxwell tension and the total pressure gradient surrounding the DF and found that the imbalance between the curvature force density and the pressure gradient force density would lead to the flux tube acceleration. Ions, essentially nonadiabatic in the magnetotail, can be directly accelerated by the electric field produced by earthward convection of the front, such as due to surfing acceleration or shock drift acceleration (Birn et al., 2012, 2013; Ukhorskiy et al., 2013; Artemyev et al., 2014). Electrons, comparatively adiabatic over most of their orbits, can be accelerated through betatron and Fermi process (Birn et al., 2004, 2012). It is noticed that the magnetic field amplitude behind DF is much greater than that ahead of it, Zhou et al. (2011, 2014) obtained that the earthward moving front can reflect and accelerate ions. Ukhorskiy et al. (2013, 2017) took the magnetic field component Bz for different areas and situations into account, revealing a new robust acceleration mechanism enabled by stable trapping of ions. In most cases, ions are energized by combined actions from different acceleration mechanisms. Nevertheless, the physical processes that generate suprathermal particles are not yet fully understood.

On the simulation ground, previous two-dimensional simulations just unveil large scale physical process concerning DFs, in their models, the electric field (most of them are derived from $-\mathrm{V}\times\mathrm{B}$) is assumed to be solely in the y direction behind DFs (Ukhorskiy et al., 2012; Greco et al., 2014; Zhou et al., 2014). It has been found that the spatial scale of DFs in the dawn-dusk direction is about 1-3 R_E and its thickness is on the order of the ion inertial length (Runov et al., 2011; Schmid et al., 2011), which would be between 500 and 1000 km. In the sub-ion scale, there is an electric field directed normal to the DF. The frozen-in condition is broken at the DF and the electric field is mainly attributed by the Hall and electron pressure gradient terms, with the Hall term dominants (Fu et al., 2012b; Lu et al., 2013; Lu et al., 2015). Therefore, the Hall MHD model is necessary to obtain the Hall electric field, which may determine the electric system on DFs.

Lu et al. (2013) have successfully simulated the DF associated with interchange instability in the magnetotail and the trend of simulated physical variables are in good agreement with observations. In this paper, we improve the simulation model in order to study how the Hall electric field on DFs acts on the particle trajectories and ion energizations. Since the DF would be produced by temporal evolution of interchange instability self-consistently through our Hall MHD simulation, it would be meaningful to understand the ion acceleration mechanism associated with the interchange instability in the magnetotail.

Theoretical and Numerical Model

Numerical simulations have proved that the existence of interchange instability triggered by the tailward gradient of thermal pressure and the earthward magnetic curvature force is a possible generation mechanism of the DFs in the magnetotail (Guzdar et al., 2010). Based on the Hall MHD model associated with interchange instability (Lu et al., 2013), we conducted test particle simulations to track ion trajectories backward in time by running the simulation with positive time step then check the time history of the trajectories of selected particles.

Our simulation was performed by two steps, the first is to establish a more realistic DF to get particle motion background. The other is to place test particles and track their trajectories.

The simulation coordinate system is defined with the x-axis pointing away from the Earth, the y-axis pointing from dusk to dawn, and the z-axis pointing northward (Guzdar et al., 2010, Figure 1). The breaking of the earthward flow together with the curvature of the vertical field leads to an effective gravity g away from the earth. Dimensional units are based on a magnetic field of 10 nT, the Alfven velocity of 500 km/s, and reference length of 1 R_E leading to a time unit of ~13 s, an electric field of 5 mV/m.

The dimensionless model with an effective gravity is as follows:

$$\frac{\partial}{\partial t}\begin{bmatrix}\rho\\ \rho\mathbf{U}\\ \mathbf{B}\\ \rho e_t\end{bmatrix}+\nabla\cdot\begin{bmatrix}\rho\mathbf{U}\\ \rho\mathbf{U}\mathbf{U}+P\mathbf{I}-\dfrac{\mathbf{B}\mathbf{B}}{\mu_0}\\ \mathbf{U}\mathbf{B}\text{-}\mathbf{B}\mathbf{U}\\ (\rho e_t+P)\mathbf{U}-\dfrac{\mathbf{B}}{\mu_0}(\mathbf{U}\cdot\mathbf{B})\end{bmatrix}=\begin{bmatrix}0\\ \mathbf{g}\\ 0\\ \mathbf{g}.\mathbf{U}\end{bmatrix}+ d_i\begin{bmatrix}0\\ 0\\ -\dfrac{1}{\mu_0}\nabla\times\left(\dfrac{\nabla\times\mathbf{B}\times\mathbf{B}}{\rho}\right)\\ -\dfrac{1}{\mu_0^2}\mathbf{B}\cdot\left[\nabla\times\left(\dfrac{\nabla\times\mathbf{B}\times\mathbf{B}}{\rho}\right)\right]\end{bmatrix}+d_i\begin{bmatrix}0\\ 0\\ -\dfrac{1}{\mu_0}\nabla\times\left(\dfrac{\nabla p_e}{\rho}\right)\\ -\dfrac{1}{\mu_0^2}\mathbf{B}\cdot\left[\nabla\times\left(\dfrac{\nabla p_e}{\rho}\right)\right]\end{bmatrix} \quad (1)$$

Where $\mathrm{P} = \mathrm{p} + \boldsymbol{B}^2/2\mu_0$, $\mathbf{U}$ and $\mathbf{B}$ are velocity vector and magnetic field vector, respectively, $\rho e_t = \rho\boldsymbol{U}^2/2 + p/(\gamma-1) + \boldsymbol{B}^2/2\mu_0$, $\mathbf{g} = [\beta\rho g_x/2\,,0,0]^T$, β is plasma beta, g_x is the effective gravitational force in x direction. In equation (1), the second and third terms on the right-hand side represent the Hall effect and the electron pressure gradient, respectively. In our present numerical cases, we postulate that plasma is under isothermal conditions with an isothermal equation of state $\mathrm{p} = \beta\rho/2$ and take the adiabatic exponent $\gamma = 5/3$. The ion inertial length $d_i = (m_i/\mu_0 e^2 Z^2 L^2 n_i)^{1/2}$, given the reference length L = 1 R_E, the dimensionless ion inertial length is taken as

$d_i \approx 0.1$. Electron pressure p_e is taken as $p/6$, because the ion temperature is 5 times that of electron temperature (Baumjohann et al., 1989; Artemyev et al., 2011).

As for initial conditions, the quasi-stationary equilibrium built by the plasma pressure and effective gravity g (see equation (2)) (Guzdar et al. 2010 and Lu et al. 2013, 2015) is theoretically reasonable.

$$\hat{g}\frac{\beta}{2}\rho = \frac{\partial}{\partial x}\left(\frac{\beta}{2}\rho + \frac{B_z^2}{2}\right) \tag{2}$$

It should be noticed that the dawn-dusk and earthward electric field components averagely, increase to ~5 mV/m along with the transient Bz increase and in some events, the electric field increase exceeded 10 mV/m (Runov et al., 2009, 2011; Schmid, D., et al. 2016). However, the electric fields calculated by the Hall MHD model in Lu et al. (2013) are smaller than the observations (see Lu et al., 2013, for a typical dipolarization event at x = -10 R_E in the equatorial plane, they set B_0 = 15 nT, leading to Bz changed from 10.2 nT to 16.8 nT after DF propagation. The electric field components E_x and E_y are both less than 3 mV/m). So, it is reasonable that we improve the initial conditions to obtain a realistic electric field, which plays a vital important role in ion energization.

We take the initial conditions as follows:

$$\rho(x) = \frac{1}{2}(\rho_L + \rho_R) - \frac{1}{2}(\rho_L - \rho_R)\tanh\left(\frac{x}{l}\right) \tag{3}$$

$$
\begin{cases} B_Z(x) = 0.28x + 0.7535 & (\mathrm{x} \leq -0.38) \\ B_Z(x) = 1.5 + \tanh\left(\frac{x}{0.3}\right) & (-0.38 < x < 0.4) \\ B_Z(x) = 0.14x + 2.314 & (\mathrm{x} \geq 0.4) \end{cases} \tag{4}
$$

Given the generalized Ohm's law, we use a piecewise function to describe Bz so as to obtain a strong electric field. In equation (3), $\rho_L = 2$ and $\rho_R = 1$ are the density closer to and away from the Earth, respectively and the characteristic scale l = 0.2 R_E. The numbers of grid cells in x and y directions are set 301 and 201, respectively.

We solved equation (1) by adopting the second-order upwind total variation diminishing scheme. The simulation box is 4 R_E and 1.5 R_E in the direction of x and y, respectively. The x boundary is assumed to be zero for all perturbed quantities and the y boundary is to be periodic.

As the second simulation step, the control equations for ion motion should be given. Typically, the drift approximation breaks down in terms of ion motion in magnetotail. The dimensionless equations of motion are given by

$$
\begin{cases} \frac{d\boldsymbol{r}}{dt} = \boldsymbol{u} \\ \frac{d\boldsymbol{u}}{dt} = \alpha(\boldsymbol{E} + \boldsymbol{V} \times \boldsymbol{B}) \end{cases} \tag{5}
$$

where $\boldsymbol{r}$ is the particle position, $\boldsymbol{u}$ is the particle velocity, the dimensional parameter $\alpha = \frac{1}{d_i} \approx 10$.

Simulation Results

From 0s to 221s, the simulation experienced a pre-onset phase, during which the DF formed as a consequence of effective gravity g interaction with plasma density gradient. In order to be more realistic, we set up the time interval from 221s to 286s as the acceleration period of the particles. Figure 1 shows the evolution of the electric field in the z = 0 plane and black lines indicate streamlines, one can clearly see that the DF moves toward the Earth as time passes by. From Figure 1b it can be seen that the earthward flows coexisted with the tailward flows of the dawn and dusk edges, as a consequence two vortex flow pattern appeared. Figure 1 also shows that the electric field components E_x and E_y are both normal to the front, which is consistent with the observation and simulation (Fu et al., 2012b; Lu et al., 2013). It should be noticed that the total electric field E is asymmetrically distributed on the DF, with a stronger dawnside electric field in Figure 1. This asymmetry can be interpreted as a subsequence of Lorentz force, according to the Hall electric field. Consequently, the Lorentz force along the tangent plane of DF associated with the motions of the decoupled ions leads to the asymmetry of the "mushroom" pattern (Lu et al. 2013).

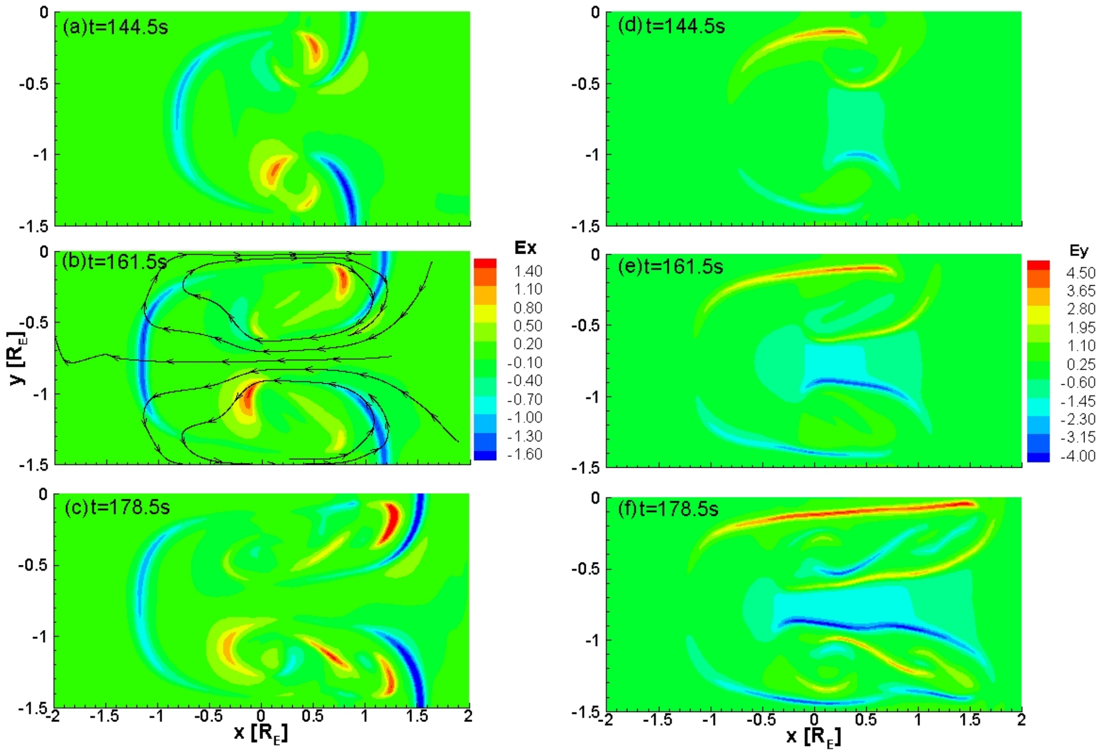

Figure 1. Evolution of the electric field E_x (a-c) and E_y (d-f), black line in (b) indicate streamlines

At t = 144.5s, we numerically distribute test particles (80000 ions in total) around the DF (the launch region with x = -0.9 R_E ~ -0.4 R_E, y = -1.46 R_E ~ -0.04 R_E) with the initial power law energy distribution $F \sim (1 + h/\kappa T_0)^{-\kappa-1}$(we take $\kappa = 5$, $T_0 = 1.5\ keV$ and h from 1 keV to 10 keV) (Artemyev et al., 2015). Figure 2 exhibits the spatial distribution of ions at a given moment. The energy of particles is marked with color and black lines indicate the position of DFs. As time passes by, the ions behind the DF accelerate and transport to the dawn flank of the DF, resulting in the reduction of the ion density behind the DF. It should be pointed that the ions will remain stationary at the boundary once they move to the simulated boundary. We investigated the characteristics of ions trajectories and found that the behaviors of ions consist of two parts (not shown), one is forced by the electric field Ex at the leading edge of the front, resulting in earthward motion and dawnward drift. Another is due to the electric field E_y at the dawn flank of the DF, leading to tailward drift. These results are consistent with observations and simulations (Nakamura et al., 2002; Greco et al., 2014; Zhou et al., 2011, 2014). Therefore, the electric field on the DF (Figure 1a), mainly produced by Hall term and always normal to the front (Fu et al., 2012b; Lu et al., 2013), makes the particles move in the way described above. Statistical analysis of the ions energy in Figure 2 indicates that the maximum energy is about 12 keV. In order to better distinguish particles from different energy, we assumed that the ions with the final energy greater than 6 keV are high-energy particles.

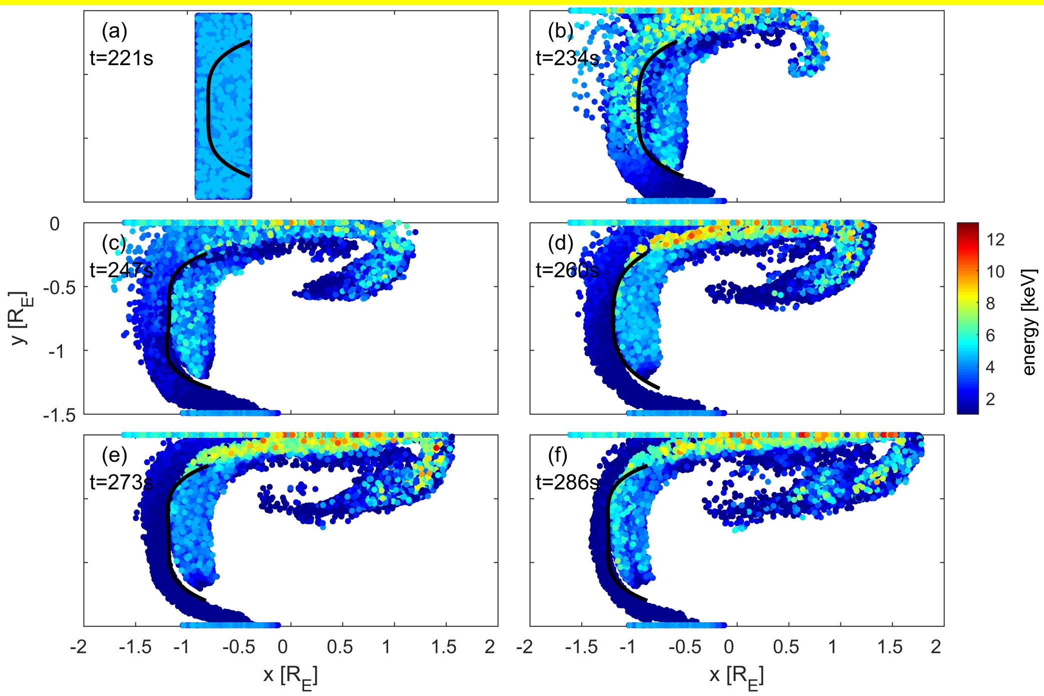

Figure 2. Test particle simulations of ion energization at the DF, particle

energy is indicated with color and black line represents the position of the DF

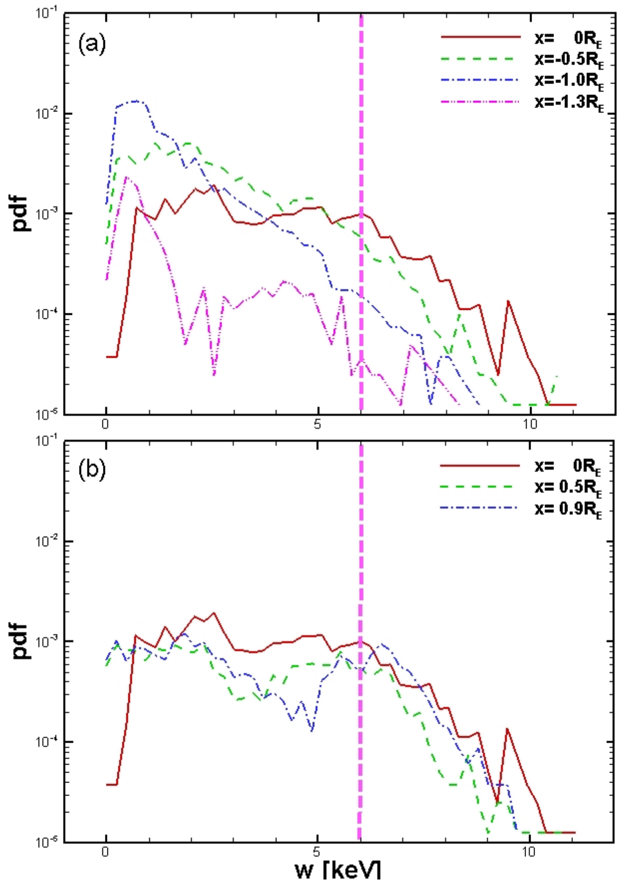

Figure 3. PDFs of particle energy computed at the region of (a) x < 0 R_E and (b) x > 0 R_E. The red dotted line mark the high energy demarcation line 6 keV.

Figure 3 gives the probability density function (PDF) of particle energy at different x positions at final time. In order to better distinguish the curves of different x distances, we show the results in two figures according to different region in x direction. It can be seen from Figure 3b that the high-energy particles are assembled in the region of x > -0.5 R_E whereas Figure 3a shows that the low energy (~ 2keV) ions are concentrated in the region of x < -0.5 R_E. At x = 0 R_E, ion energy is evenly distributed between 1 keV and 6 keV practically. In combination with Figure 2, we can further obtain that almost all the high-energy particles gathered in the dawnside of x > -0.5 R_E region. It implies that ion acceleration is more effective at the dawnside of DF.

To have a statistical description of high-energy ions, we picked out high-energy particles from the total number. The simulation results are shown in Figure 4 with ions energy marked with different color. It appears that high energy particles, accounting for 7.45 percent, mainly gathering at the dawnside of the DF.

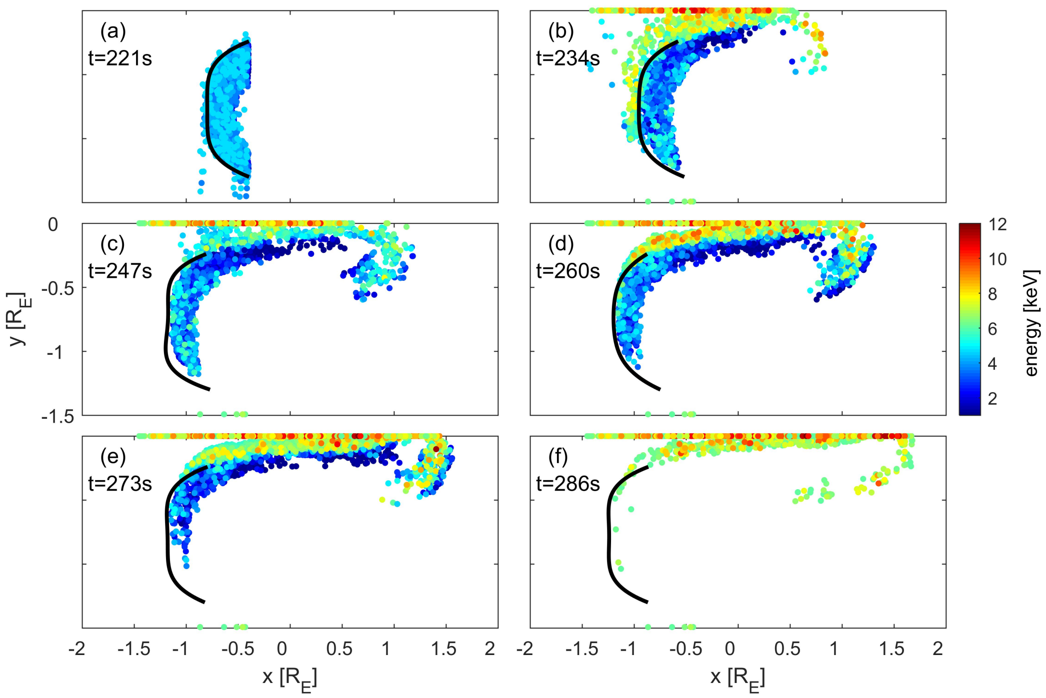

Figure 4. Snapshots of high-energy ions at specific moment of the simulation, black line represents the pre-region position of the DF

Figure 4a shows that the initial position of high-energy particles is roughly an asymmetric semicircle whereas the dawnside area is wider than the duskside, which means that more ions are accelerated in the dawnside than in the duskside. Compared with Figure 2, however, we can intuitively infer that ions with initial positions ahead of or behind and away from the front would not obtain great energization. The ions with initial positions ahead of the front are forced by the Ex of pre-DF region and they move earthward and dawnward with a larger gyration radius due to smaller ambient magnetic Bz, thus can't be accelerated by the dawnside electric field $E_{y.}$ The ions with initial positions behind the front move with it and always stay behind the DF during the whole evolution period of DF. As a result, there exist no strong fields to energized ions. That is to say, only particles which diverted to the dawnside region closer to the front can be effectively accelerated.

In a previous paper, Zhou et al. (2014) inferred that the more energized DF-reflected ions originating from the duskside of the DF would be able to reach farther into the ambient. In their model the ions would have been accelerated more significantly in the DF duskside than in its dawnside which is due to the y displacements behind the convex DF (Zhou et al., 2014 Figure 3). However, observations and numerical simulations indicate that the convective electric field behind the front is smaller than the Hall term on the DF on the spatial scale of ion inertial length (Fu et al., 2012b). Therefore, the explanation based on the convective electric field E_y was inappropriate in oue model. Figure 4 has already illustrated that the ion acceleration process is on the dawnside. In addition, statistical analysis of 5961 high-energy ions indicates that 2004 ions were traced to the duskside of the DF, about 34 % of the total high-energy particles. The source area of ions reaches closer to the Earth, as shown in Figure5.

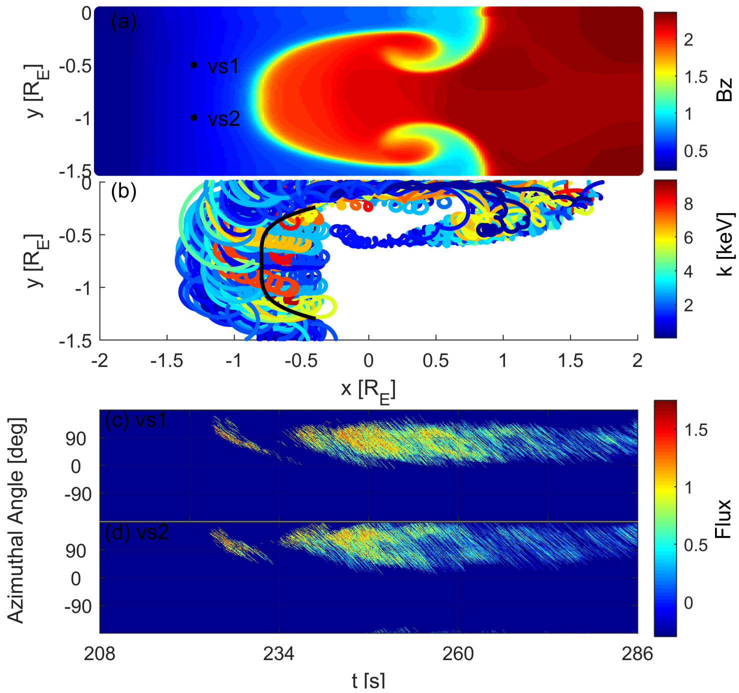

Figure 5. Simulation results of ion differential energy fluxes in the 1-20 keV energy range at different location. (a) Positions of virtual satellites. (b) Ions with initial positions on different y locations moving with the dipolarization front, the DF at t = 221 s was marked with black solid line. Kinetic energy at finial moment is marked with color. (c and d) Differential energy fluxes at dawnside (vs1) and duskside (vs2), respectively, as the functions of equatorial azimuthal angle and time.

The dark spots in Figure 5a mark the locations of the virtual satellites. Figure 5c and 5d show the distribution of differential energy flux as the function of equatorial azimuthal angle and time at the duskside and dawnside of the DF respectively. Ion trajectories with initial positions along different y locations in Figure 5c and 5d are plotted in Figure 5b where the DF at t = 221 s is set as baseline and marked with black solid line. Kinetic energy at finial moment is indicated with color.

It is obviously seen in Figure 5 that the duskside ions tend to move to dawn at the front (Figure 5d, $90^{\circ} < \theta < 180^{\circ}$), while the dawnside ones divert toward tailward (Figure 5c, $0^{\circ} < \theta < 90^{\circ}$). This finding is similar to the fluxes of 78-300 keV ions in Birn et al. (2015). At about t = 221s ~153s, the particles with higher initial energy ahead of the front have large radius of gyration and those particles are minor affected by the smaller initial electric field, therefore they are almost simultaneously observed (Figure 5b and 5d). While at t > 234s ions with the initial position at duskside would be able to reach farther into the ambient, which is consistent with the results of Zhou et al. (2014) and Birn et al. (2015). On the other hand, the earlier observed ions are not the most energized ions compared with high-energy counterparts in our model, which is opposite to Zhou's conclusion. It can be easily understood by considering the Hall electric field. The small electric field near the duskside of the front allows particles to drift toward earthward and dawnward for a long time, whereas the high one close to dawnside forces ions to drift tailward quickly during the period that particles obtain most energy (Figure 4).

In order to study how the Hall field E_y on the dawnside of DF accelerate ions, we choose one typical ion to track its trajectory, which is initiated at x = -0.7 R_E, y = -0.86 R_E behind the DF with an azimuth angle of 14.58° and initial kinetic energy of 1 keV. Its final kinetic energy is 12 keV, as shown in Figure 6. Figure 7 demonstrates the evolution of ion positions and energy and Figure 8 shows the local Bz, E_x, E_y seen by this particle. During the beginning period from 221s to 247s, the ion moves earthward together with the front and meanwhile dawnward in the frame of the moving front. During this period, the ion gains very little energy. Even though the Ex component of electric field accelerates the ion along its earthward motion, the deceleration by the E_y component keeps the ion energy almost unchanged. When t = 249.6s, the ion arrives at the dawnside of the DF, where the Hall electric field is very strong. After a sharp energization for about 5 seconds, the ion kinetic energy increase to ~ 5 keV (Figure 7b and 7c, the weaker E_x works to reduce the energy by about 3.7 keV and the stronger E_y increases the energy by about 9 keV). As shown in Figure 6 and 7, when t > 253.8 s, the ion kinetic energy gradually increases, which can be interpreted based on the fact that the y-displacement δy^+ (corresponding to the energy increase) is larger than δy^- (corresponding to the energy reduction) in the case where E_y component is almost constant. Since the ions arrive at the ambient of dawnward DF, the magnitude of magnetic field is increase, which results in a high δy^{+}.Figure 8 shows the time history of the local Bz, E_x, E_y.

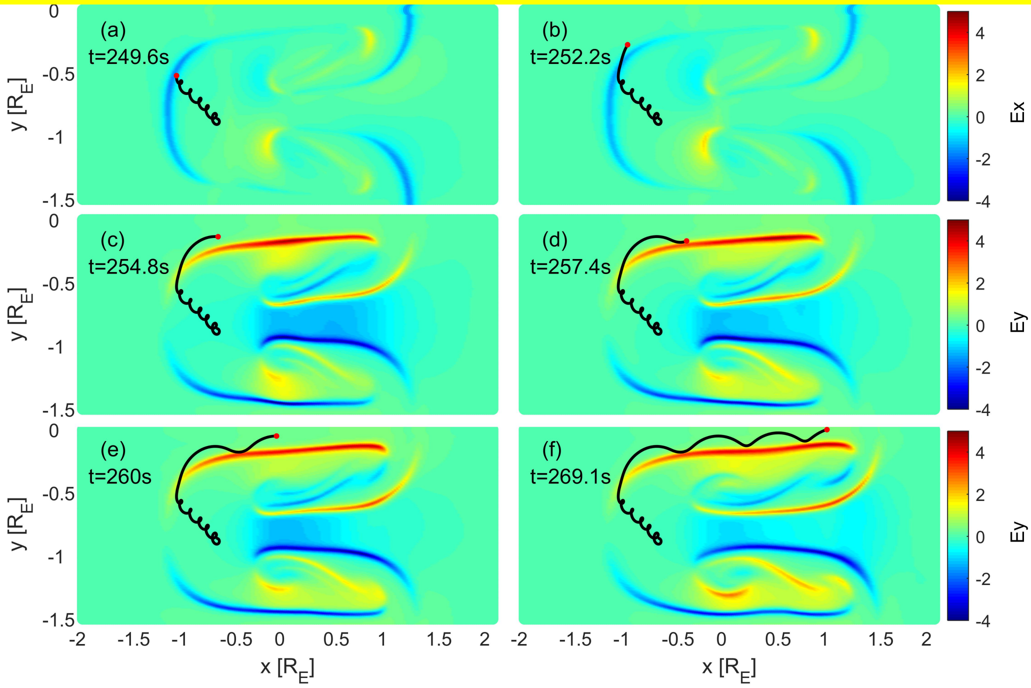

Figure 6. Orbits of an ion with the initial energy 1 keV and final energy 5.54 keV, traced from x = -0.7 R_E, y = -0.86 R_E at different moments. The locations of ion are shown as red dots superposed on snapshots of the background Hall electric field E_x (a-b) and E_y (c-f).

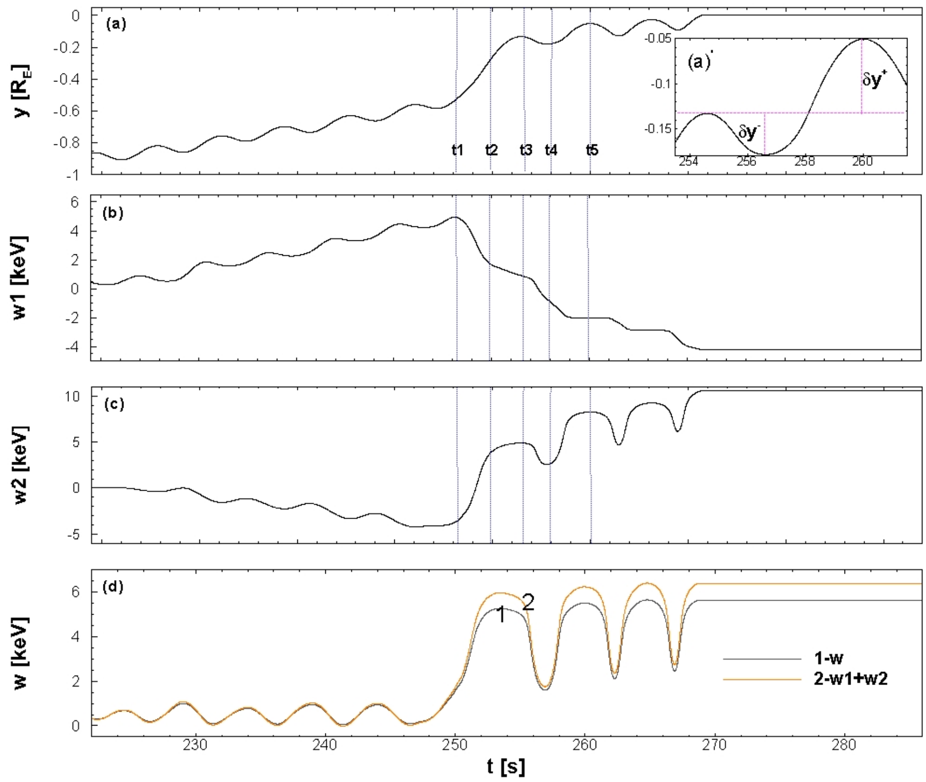

Figure 7. Physical quantities of ion as the function of time with blue dotted lines index specific moment. (a), (a’) Y position and its partial enlarged detail, red dotted line is the reference line. (b, c) Energization produced by E_x and E_y, respectively. (d) Kinetic energy and numerical summation of w1 and w2 display with orange and black line, respectively. The label of t1 to t5 correspond to 249.6s, 252.2s, 254.8s, 256.9s and 260s respectively.

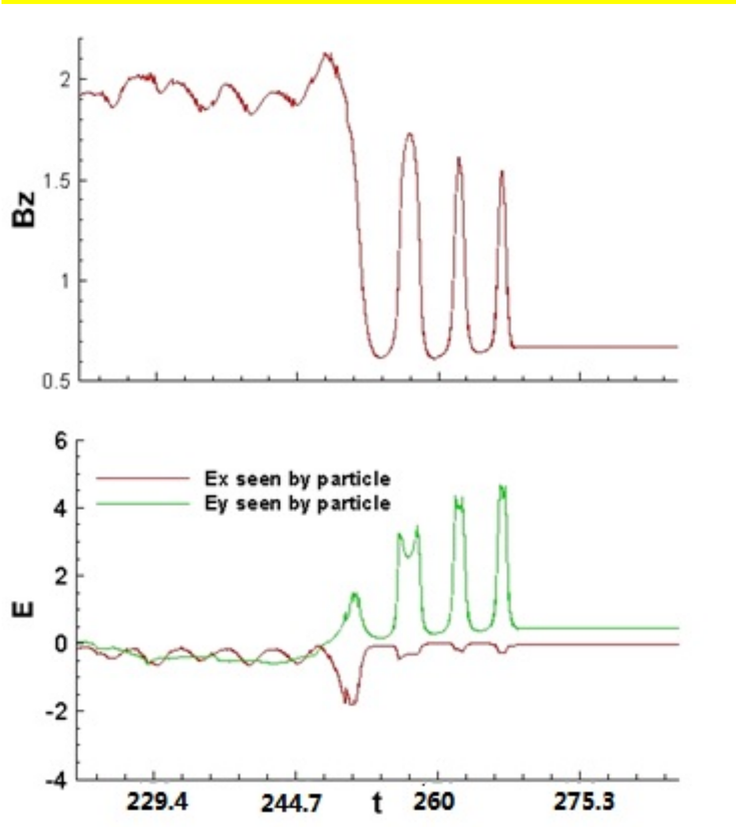

Figure 8. The time history of the local Bz, E_x, E_y

Summary and Discussion

In this paper, we used a test particle simulation to investigate ion acceleration at dipolarization fronts (DFs) produced by interchange instability in the magnetotail. The Hall MHD model was improved by applying the realistic initial conditions to obtain the fields which are better consistent with observation.

It should be noticed that our test particle is 2D without the motion in the z direction along the field line. So we only study the ions with 90-degree pitch angle. Test particles were settled in both the pre-DF and post-DF region, most of them exhibited earthward and dawnward drift and then diverted tailward. It is found that ions with the initial position at duskside would be able to reach farther into the ambient plasma, which has been also proofed by Zhou et al. (2014) and Birn et al. (2015). Statistical analysis shows that the high-energy particles are mainly assembled in the dawnside of x > -0.5 R_E region, which suggests the dawnside region of the DF is the main area for particle acceleration.

Numerical simulation results indicate that the ions initially settled behind the front may obtain higher energization. In order to explain how the Hall electric field influence ions, we tracked the trajectory of particular ions in the ion-scale electric field. As expected, the E_y component at the dawn flank of DF plays an important role in the acceleration of ion. Although the Ex component in the pre-DF region constitutes a potential drop of ~ 1 keV across the DF as reported by Fu et al., (2012b), the energy enhancement would be offset on their way out toward the magnetotail due to the E_y component. The spatial and temporal properties of E_y component are critical factors for particle acceleration (Greco et al., 2014; Birn et al., 2013, 2015; Artemyev et al., 2015; Ukhorskiy et al., 2017). In contrast to the results from other MHD model, it makes sense in our self-consistent Hall MHD simulation that the accelerating electric field is the E_y component of the Hall electric field on the dawnside of the front instead of the convection electric field E_y behind the front in their model.

Our test particle simulation can well reproduce the direct acceleration process generated by the Hall field. Nevertheless, it should be pointed out that the ion acceleration mechanisms such as Fermi acceleration and resonance acceleration can also provide powerful ion energization with tens of keV to hundreds of keV (Fu et al.,2011; Artemyev et al., 2012), which is not discussed in this paper. Still, there is no doubt that our study suggests that the dawn flank dusk-dawn electric field plays an essential role in ions energization.

Acknowledgements

Our work was supported by the National Natural Science Foundation of China (NSFC) under grants 41474144, 41674176, and 41474124, and the fund of the Lunar and Planetary Science Laboratory, Macau University of Science and Technology - Partner Laboratory of Key Laboratory of Lunar and Deep Space Exploration, Chinese Academy of Sciences (FDCT No. 039/2013/A2). The simulation data will be made available up on request by contacting Haoyu Lu.

Reference

Angelopoulos, V., Kennel, C. F., Coroniti, F. V., Pellat, R., Kivelson, M. G., Walker, R. J., Russell, C. T., Baumjohann, W., Feldman, W. C., and Gosling, J. T.: Statistical characteristics of bursty bulk flow events, J. Geophys. Res., 99(A11), 21,257–21,280, 1994.

Artemyev, A. V., Liu, J., Angelopoulos, V., and Runov, A.: Acceleration of ions by electric field pulses in the inner magnetosphere, J. Geophys. Res. Space Physics, 120, 4628–4640, 2015.

Artemyev, A. V., Lutsenko, V. N., and Petrukovich, A. A.: Ion resonance acceleration by dipolarization fronts: Analytic theory and spacecraft observation, Ann. Geophys., 30, 317–324, 2012.

Artemyev, A. V., Baumjohann, W., Petrukovich, A. A., Nakamura, R., Dandouras, I., and Fazakerley, A.: Proton/electron temperature ratio in the magnetotail, Ann. Geophys., 29, 2253–2257, 2011.

Artemyev, A. V., Zimbardo, G., A. Ukhorskiy, Y., and Fujimoto, M.: Preferential acceleration of heavy ions in the reconnection outflow region. Drift and surfatron ion acceleration, Astron. Astrophys., 562, A58, 2014.

Baumjohann, W., Paschmann, G., and Cattell, C. A.: Average plasma properties in the central plasma sheet, J. Geophys. Res., 94, 6597–6606, 1989.

Birn, J., Runov, A., and Hesse, M.: Energetic ions in dipolarization events, J. Geophys. Res. Space Physics, 120, 7698–7717, 2015.

Birn, J., Artemyev, A. V., Baker, D. N., Echim, M., Hoshino, M., and Zelenyi, L. M.: Particle acceleration in the magnetotail and aurora, Space Sci. Rev., 173, 49–102, 2012.

Birn, J., Thomsen, M. F., and Hesse M.: Electron acceleration in the dynamic magnetotail: Test particle orbits in three-dimensional MHD simulation fields, Phys. Plasmas, 11, 1825–1833, 2004.

Birn, J., Hesse, M., Nakamura, R., and Zaharia, S.: Particle acceleration in dipolarization events, J. Geophys. Res. Space Physics, 118,1960–1971, 2013.

Birn, J., Nakamura, R., Panov, E. V., and Hesse, M.: Bursty bulk flows and dipolarization in MHD simulations of magnetotail reconnection, J. Geophys. Res., 116, A01210, 2011.

Fu, H. S., Khotyaintsev, Y. V., Vaivads, A., André, M., and Huang, S. Y.: Occurrence rate of earthward-propagating dipolarization fronts, Geophys. Res. Lett., 39, L10101, 2012a.

Fu, H. S., Khotyaintsev, Y. V., Vaivads, A., André, M., and Huang, S. Y.: Electric structure of dipolarization front at sub-proton scale, Geophys. Res. Lett., 39, L06105, 2012b.

Fu, H. S., Khotyaintsev, Y. V., André, M., and Vaivads, A.: Fermi and betatron acceleration of suprathermal electrons behind dipolarization fronts, Geophys. Res. Lett., 38, L16104, 2011.

Fu, H. S., Cao, J. B., Khotyaintsev, Y. V., Sitnov, M. I., Runov, A., Fu, S. Y., Hamrin, M., André, M., Retinò, A., Ma, Y. D., Lu, H. Y., Wei, X. H., and Huang, S. Y.: Dipolarization fronts as a consequence of transient reconnection: In situ evidence, Geophys. Res. Lett., 40, 6023–6027, 2013.

Ge, Y. S., Raeder, J., Angelopoulos, V., Gilson, M. L., and Runov, A.:

Interaction of dipolarization fronts within multiple bursty bulk flows in global MHD simulations of a substorm on 27 February 2009, J. Geophys. Res., 116, A00I23, 2011.

Greco, A., Artemyev, A., and Zimbardo, G.: Proton acceleration at two-dimensional dipolarization fronts in the magnetotail, J. Geophys. Res. Space Physics, 119, 8929–8941, 2014.

Guzdar, P. N., Hassam, A. B., Swisdak, M., and Sitnov, M. I.: A simple MHD model for the formation of multiple dipolarization fronts, Geophys. Res. Lett., 37, L20102, 2010.

Huang, S. Y., Yuan, Z. G., Ni, B., Zhou, M., Fu, H. S., Fu, S., Deng, X. H., Pang, Y., Li, H. M., Wang, D. D., Li, H. M., Yu, X. D.: Observations of large-amplitude electromagnetic waves and associated wave-particle interactions at the dipolarization front in the Earth's magnetotail: A case study, J. Atmos. Sol. Terr. Phys., 129, 119–127, 2015.

Kiehas, S. A., Semenov, V. S., Kubyshkina, M. V., Angelopoulos, V., Nakamura, R., Keika, K., Ivanova, V. V., Biernat, H. K., Baumjohann, W., Mende, S., Magnes, W., Auster, U., Fornaçon, K.-H., Larson, D., Carlson, C. W., Bonnell, J., McFadden, J.: First application of a Petschek-type reconnection model with time-varying reconnection rate to THEMIS observations, J. Geophys. Res., 114, A00C20, 2009.

Li, S.-S., Angelopoulos, V., Runov, A., Zhou, X.-Z., McFadden, J., Larson, D., Bonnell, J., and Auster, U.: On the force balance around dipolarization fronts within bursty bulk flows, J. Geophys. Res., 116, A00I35, 2011.

Lu, H. Y., Cao, J. B., Zhou, M., Fu, H. S., Nakamura, R., Zhang, T. L., Khotyaintsev, Y. V., Ma, Y. D., and Tao, D.: Electric structure of dipolarization fronts associated with interchange instability in the magnetotail, J. Geophys. Res. Space Physics, 118, 2013.

Lu, H. Y., Cao, J. B., Ge, Y. S., Zhang, T. L., Nakamura, R., and Dunlop, M. W.: Hall and finite Larmor radius effects on the dipolarization fronts associated with interchange instability, Geophys. Res. Lett., 42, 2015.

Lu, H.Y., Li, Y., Cao, J., Ge, Y., Zhang, T., and Yu, Y.: Numerical simulation on the multiple dipolarization fronts in the magnetotail, Phys. Plasmas 24, 102903 2017.

Nakamura, R., Baumjohann, W., Klecker, B., Bogdanova, Y., Balogh, A., Remé, H., Bosqued, J., Dandouras, I., Sauvaud, J., Glassmeier, K., Kistler, L., Mouikis, C., Zhang, T., Eichelberger, H. and Runov, A.: Motion of the dipolarization front during a flow burst event observed by Cluster, Geophys. Res. Lett., 29(20), 1942, 2002.

Nakamura, R., Retinò, A., Baumjohann, W., Volwerk, M., Erkaev, N., Klecker, B., Lucek, E. A., Dandouras, I., André, M., Khotyaintsev, Y.: Evolution of dipolarization in the near-Earth current sheet induced by

Earthward rapid flux transport, Ann. Geophys., 27, 1743–1754,2009.

Nakamura, R., Baumjohann, W., Panov, E., Volwerk, M., Birn, J., Artemyev, A., Petrukovich, A. A., Amm, O., Juusola, L., Kubyshkina, M. V., Apatenkov, S., Kronberg, E. A., Daly, P. W., Fillingim, M., Weygand, J. M., Fazakerley, A., Khotyaintsev, Y.: Flow bouncing and electron injection observed by Cluster, J. Geophys. Res. Space Physics, 118, 2055–2072, 2013.

Ohtani, S. I., Shay, M. A., and Mukai, T.: Temporal structure of the fast convective flow in the plasma sheet: Comparison between observations and two-fluid simulations, J. Geophys. Res., 109, A03210, 2004.

Pritchett, P. L., and Coroniti, F. V.: Structure and consequences of the kinetic ballooning/interchange instability in the magnetotail, J. Geophys. Res. Space Physics, 118, 146-159, 2013.

Runov, A., Angelopoulos, V., Sitnov, M. I., Sergeev, V. A., Bonnell J., McFadden, J. P., Larson, D., Glassmeier, K.-H., and Auster, U.: THEMIS observations of an earthward-propagating dipolarization front, Geophys. Res. Lett, 36, L14106, 2009.

Runov, A., Angelopoulos, V., Zhou, X.-Z., Zhang, X.-J., Li, S., Plaschke, F., and Bonnell, J.: A THEMIS multicase study of dipolarization fronts in the magnetotail plasma sheet, J. Geophys. Res., 116, A05216, 2011.

Schmid, D., et al. (), A comparative study of dipolarization fronts at

MMS and Cluster, Geophys. Res. Lett., 43, 6012–6019, 20160.

Schmid, D., Volwerk, M., Nakamura, R., Baumjohann, W., and Heyn, M.: A statistical and event study of magnetotail dipolarization fronts, Ann. Geophys., 29, 1537–1547, 2011.

Sitnov, M. I., Swisdak, M., and Divin, A. V.: Dipolarization fronts as a signature of transient reconnection in the magnetotail, J. Geophys. Res., 114, A04202, 2009.

Ukhorskiy, A. Y., Sitnov, M. I., Merkin, V. G., and Artemyev, A. V.: Rapid acceleration of protons upstream of earthward propagating dipolarization fronts, J. Geophys. Res. Space Physics, 118, 4952–4962, 2013.

Ukhorskiy, A. Y., Sitnov, M. I., Merkin, V. G., Gkioulidou, M., and Mitchell, D. G.: Ion acceleration at dipolarization fronts in the inner magnetosphere, J. Geophys. Res. Space Physics, 122, 3040–3054, 2017.

Zhou, M., Huang, S.-Y., Deng, X.-H., and Pang, Y.: Observation of a sharp negative dipolarization front in the reconnection outflow region, Chin. Phys. Lett., 28(10), 109402, 2011.

Zhou, X.-Z., Angelopoulos, V., Liu, J., Runov, A., and Li, S.-S.: On the origin of pressure and magnetic perturbations ahead of dipolarization fronts, J. Geophys. Res. Space Physics, 119,211–220, 2014.

Zhou, X.-Z., Angelopoulos, V., Sergeev, V. A., and Runov, A.:

Accelerated ions ahead of earthward propagating dipolarization fronts, J. Geophys. Res., 115, A00I03, 2010.

Zhou, X.-Z., Angelopoulos, V., Sergeev, V. A., and Runov, A.: On the nature of precursor flows upstream of advancing dipolarization fronts, J. Geophys. Res., 116, A03222, 2011.